Published in final edited form as:
ACS Nano. 2009 October 27; 3(10): 3165–3174. doi:10.1021/nn900649v.

HFT-T, a Targeting Nanoparticle, Enhances Specific Delivery of Paclitaxel to Folate Receptor-Positive Tumors

Xu Wang[1,#], **Jun Li**[2,#], **Yiqing Wang**[2], **Kwang Jae Cho**[1], **Gloria Kim**[2], **Ada Gjyrezi**[3], **Lydia Koenig**[1], **Paraskevi Giannakakou**[3], **Hyung Ju C. Shin**[4], **Mourad Tighiouart**[5], **Shuming Nie**[2], **Zhuo (Georgia) Chen**[1], and **Dong M. Shin**[1,*]

[1]Department of Hematology and Medical Oncology, Winship Cancer Institute, Emory University School of Medicine Atlanta, GA

[2]Department of Biomedical Engineering, Emory University School of Medicine Atlanta, GA

[3]Department of Pharmacology, Weill Medical College of Cornell University. New York, NY

[4]Quest Diagnostics, Atlanta, GA

[5]Department of Biostatistics & Bioinformatics, Winship Cancer Institute, Emory University Rollins School of Public Health Atlanta, GA

Abstract

Non-specific distribution of chemotherapeutic drugs (such as paclitaxel) is a major factor contributing to side effects and poor clinical outcomes in the treatment of human head and neck cancer. To develop novel drug delivery systems with enhanced efficacy and minimized adverse effects, we synthesized a ternary conjugate heparin-folic acid-paclitaxel (HFT), loaded with additional paclitaxel (T). The resulting nanoparticle, HFT-T, is expected to retain the antitumor activity of paclitaxel and specifically target folate receptor (FR)-expressing tumors, thereby increasing the bioavailability and efficacy of paclitaxel. *In vitro* experiments found that HFT-T selectively recognizes FR-positive human head and neck cancer cell line KB-3-1, displaying higher cytotoxicity compared to the free form of paclitaxel. In a subcutaneous KB-3-1 xenograft model, HFT-T administration enhanced the specific delivery of paclitaxel into tumor tissues and remarkably improved antitumor efficacy of paclitaxel. The average tumor volume in the HFT-T treatment group was 92.9±78.2mm^3 *vs* 1670.3±286.1mm^3 in the mice treated with free paclitaxel. Furthermore, paclitaxel tumors showed a resurgence of growth after several weeks of treatment, but this was not observed with HFT-T. This indicates that HFT-T could be more effective in preventing tumors from developing drug resistance. No significant acute *in vivo* toxicity was observed. These results indicate that specific delivery of paclitaxel with a ternary structured nanoparticle (HFT-T) targeting FR-positive tumor is a promising strategy to enhance chemotherapy efficacy and minimize adverse effects.

Keywords

Targeting nanoparticle; specific drug delivery; folate receptor; paclitaxel; chemotherapy

[*]**Correspondence to Dong M. Shin**, Department of Hematology and Medical Oncology, Winship Cancer Institute, Emory University School of Medicine, 1365-C Clifton Rd. Atlanta, GA 30322, dmshin@emory.edu.
[#]These two authors equally contributed to this work.

Introduction

Paclitaxel is one of the most widely used chemotherapeutic agents in the clinic for the treatment of advanced solid carcinomas, such as breast, ovaries, lung, and head and neck.[1-5] However, the utility of paclitaxel is compromised by its poor aqueous solubility that necessitates its formulation with the surfactant Cremophor EL as a delivery vehicle, which can cause serious side effects including allergic reaction, nephrotoxicity, neurotoxicity, and cardiotoxity.[6] Consequently, patients who receive paclitaxel must be premedicated with steroids and antihistamines to reduce the risk of such reactions, and special non-di (2-ethylhexyl) phthalate tubing and in-line filters are required for i.v. administration.[7] Furthermore, non-specific systemic delivery of cytotoxic chemotherapeutic drugs commonly leads to dose-dependent side effects and poor therapeutic outcomes.

To overcome those limitations, many polymer-based drug delivery systems (nanoparticle formulations) have been prepared for paclitaxel delivery. A two component “binary” nanoparticle (albumin-paclitaxel or Abraxane™) is among the most developed and has been approved by the FDA for the treatment of metastatic breast cancer. This albumin-bound nanoparticle of paclitaxel showed significantly greater efficacy and lower toxicity than free paclitaxel in a phase III clinical trial.[8] However, the therapeutic benefit of binary nanoparticles with no targeting ligand is still limited. An alternative strategy to overcome the limitation is to conjugate a targeting ligand or an antibody to the nanoparticle. A variety of tumor-targeting ligands, such as antibodies, growth factors, or cytokines, have been used to facilitate the uptake of carriers into target cells.[9-19] This strategy relies on the ability of the targeting agent or ligand to bind the tumor cell surface in an appropriate manner to trigger receptor-mediated endocytosis. The therapeutic agent will thereby be delivered to the interior of the cancer cell.[20-22]

To increase the therapeutic specificity and efficacy of paclitaxel, we have developed a novel targeted polymeric nanoparticle (HFT-T), which is composed of heparin-folate-paclitaxel (HFT) conjugates loaded with paclitaxel (T) in its hydrophobic core. HFT-T exhibits improved water solubility, stability, biodegradability, and tunable drug-loading capacities. In this structure, we have chosen folic acid (FA) as a targeting agent. As a natural material, FA has several advantages as a potential targeting agent, including lower molecular weight and immunogenicity than most antibodies, relatively high stability, and ease of synthesis. Importantly, the folate receptor (FR) is highly expressed in several types of solid tumors, including ovarian, uterine, lung, breast, and head and neck cancers.[23-28] Conversely, normal tissues, most notably bone marrow tissue, lack FR expression,[26] making folate an excellent tumor-targeting moiety.

Furthermore, we have taken advantage of the natural polymer heparin, a commonly used carrier for growth factor delivery,[29, 30] to synthesize HFT-T. Heparin improves response and survival in cancer patients taking chemotherapy,[31, 32] and has an inhibitory effect on tumors that could be associated with binding of growth factors[33] and inhibition of heparinase, which is thought to be required for tumor cells to invade the vascular basement membrane.[34,35]

In this report, we present evidence to show that HFT-T has an average size of 60nm, high drug loading capability (26% w/w), facilitates specific *in vitro* and *in vivo* drug delivery into cancer cells, and significantly enhances the efficacy of paclitaxel in a human head and neck cancer xenograft model. These results suggest that targeted nanoparticles may be promising systems to achieve specific drug delivery into tumor tissues, potentially having a major impact on anticancer drug delivery to cancer patients.

RESULTS AND DISCUSSION

Synthesis and characterization of nanoparticles

Nanoparticle synthesis began by generating the binary and ternary conjugates, heparin-paclitaxel (HT) and heparin-folic acid-paclitaxel (HFT) (Fig. 1a). Paclitaxel was conjugated onto the heparin backbone through the ester linker to yield HT. For HFT synthesis, ethylene diamine-modified folic acid was conjugated onto heparin through the amide linker. Conjugates were confirmed by ^{1}H-NMR spectra (supplementary information). The content of paclitaxel and folate in HFT was 15% and 9% (w/w), respectively. To increase the loading ratio of paclitaxel, free paclitaxel was incorporated into the HT and HFT conjugates to form nanostructures (HT-T and HFT-T) by a self-assembly procedure with an efficiency above 90%. The paclitaxel content of HFT-T was increased to 26% (w/w). Comparing the ^{1}H-NMR spectra of HFT-T in *d*-DMSO and D_2O (supplementary Fig. 1) revealed that HFT-T nanoparticles formed in water were covered by a layer of FA and hydrophobic paclitaxel was shielded by heparin and FA. Transmission electron microscopy (TEM) showed that HFT-T nanoparticles were monodisperse, highly soluble and stable in aqueous solution (Fig. 1b). The HFT-T solution at 75mg/ml produced a clear liquid, which is Cremophor-free. The dynamic size of HFT-T nanoparticles measured by dynamic light scattering (DLS) was 60±10nm (Fig. 1c) and the zeta potential was −16.1±1.1mV. Since heparin was used to synthesize HFT-T, we determined the anticoagulant activity of HFT-T to be 0.23±0.08 IU/mg, only 0.13% of unconjugated heparin (178 IU/mg).

In vitro cytotoxicity of HFT-T

To compare cytotoxic activity between free paclitaxel and nanoparticle HFT-T, we performed colony formation assays using the human head and neck cancer cell lines KB-3-1 and Tu212, which express high and undetectable levels of FR, respectively. Cells were exposed to 2.5nM paclitaxel and the HFT-T and HT-T nanoparticles at a paclitaxel-equivalent dose of 2.5nM. In KB-3-1 cells, after two weeks of incubation, treatment with free paclitaxel and HT-T reduced colony formation by 50% as compared with the untreated control ($p=0.049$ and $p=0.035$, respectively), while HFT-T treatment reduced colony formation by 95% when compared with the control ($p<0.001$) (Fig. 2a,b). The suppression of colony formation by HFT-T was significantly greater than that by free paclitaxel ($p=0.009$) or HT-T ($p=0.004$), indicating that HFT-T has increased cytotoxicity *in vitro*. In contrast, HFT-T showed a similar inhibitory effect in FR-negative Tu212 cells as compared to HT-T or free paclitaxel treatment (Fig. 2c, d).

Specific *in vitro* binding and internalization of HFT-T

Since HFT-T was developed to specifically bind to FR and trigger receptor-mediated internalization in FR-positive cells, we compared the uptake of HFT-T and HT-T by KB-3-1 cells. Confocal microscopy indicated that HFT-T underwent greater cellular uptake than HT-T (Fig. 3a). The level of nanoparticle internalized in KB-3-1 cells was quantified by flow cytometry and found to be five times greater in HFT-T-treated than HT-T-treated cells (mean fluorescence 21.5±1.8 *vs.* 4.4±1.5) (Fig. 3b). To assess the specificity of FR targeting, FR-specific siRNA was used to reduce FR levels. In FR-knockdown KB-3-1 cells, HFT-T cellular uptake was decreased compared with that in cells treated with control siRNA (Fig. 3c). Quantification by flow cytometry showed that FR siRNA treatment significantly reduced cellular fluorescence intensity (6.4±1.8) compared to control siRNA treatment (19.3±1.6) (Fig. 3d). Consistently, in FR-negative Tu212 cells, HFT-T cellular uptake was less than that in FR-positive KB-3-1 cells (supplementary Fig. 2 a, b). Pre-incubation of KB-3-1 cells with FA decreased cellular uptake of HFT-T in a dose-dependent manner, indicating that HFT-T uptake may occur through FR-mediated internalization (supplementary Fig. 2 c, d).

In live-cell analysis, double fluorescence staining of HFT-T (paclitaxel-oregon green 488) and endosomes/lysosomes (LysoTracker Red DND-99) was performed to visualize the intracellular distribution of HFT-T. The majority of HFT-T was observed in endosomes/lysosomes after 2 hours of incubation, as evidenced by colocalization of green fluorescence from HFT-T and red fluorescence from LysoTracker (supplementary Fig. 3).

Accumulation of HFT-T in xenograft tumors

To compare the *in vivo* distribution of HFT-T and HT-T, we prepared near infrared dye (Cy5.5)-labeled HFT-T and HT-T nanoparticles, which provided real-time imaging of their *in vivo* biodistribution in mice after systemic injection through the tail vein (100μl of 24μM Cy5.5-labeled HFT-T or HT-T). Imaging of mice demonstrated tumor accumulation of both HFT-T and HT-T 1, 24, and 48 hours after the injection (Fig. 4a). A fluorescence signal was also observed in the bladder 1-48 hours after the injection. This signal was likely caused by small dye molecules cleaved from the nanoparticles, and/or from heparin-dye conjugates that were dissociated from the particles.

Forty-eight hours after injection, the liver, kidney, lung, heart, and spleen were collected, and all tissues were analyzed by fluorescence imaging. For both HFT-T and HT-T, the greatest fluorescence intensity was observed in the tumor compared with the other tissues (Fig. 4b). Although the signal intensity in tumor tissue was slightly higher for HFT-T than HT-T, the difference was not significant (fluorescence intensities were 462±109.1 and 368±117.5 for HFT-T- and HT-T-treated mice, respectively, $p=0.28$).

We therefore addressed whether HFT-T and HT-T nanoparticles simply accumulate around the tumor sites (outside the tumor cells) or actually enter the cells. Fluorescent dye (paclitaxel-bodipy 564)-labeled HFT-T or HT-T (200μl, 7mg/ml) was injected through the tail vein of nude mice bearing KB-3-1 tumors. Twenty-four hours post-injection, tumors were harvested and the cellular uptake of HFT-T or HT-T was evaluated by staining with anti-human CD326 (EpCAM) antibody to distinguish human carcinoma cells from the host/murine stromal cells. Fluorescence microscopy showed that fluorescent dye-labeled HFT-T predominantly accumulated within the tumor cells (Fig. 4c), while HT-T was found predominantly in the extracellular space. These data demonstrated that the specific FR-targeted nanoparticle, HFT-T, more efficiently delivered anticancer drug into tumor cells than the non-targeted nanoparticle, HT-T.

It has been proposed that the rate-limiting step for accumulation of nanoparticles in tumor tissues may be their passive extravasation through tumor vasculatures, which is affected by multiple factors including circulation time and particle size.[37] However, accumulation within the tumor microenvironment by the EPR effect may not always correlate with therapeutic outcome since cellular internalization is required for anticancer drugs to exert their biological functions inside tumor cells. HFT-T was designed to be a targeted nanoparticle, and as such demonstrated 5-fold more efficient uptake than HT-T by FR-positive KB-3-1 cells, suggesting that the conjugation of folate to the nanoparticle facilitated the targeting of HFT-T to FR-positive tumor cells. The uptake of HFT-T was decreased by FR-knockdown KB-3-1 cells or FR-negative Tu212 cells, which further supports that HFT-T specifically targets FR-expressing cells.

We next measured the uptake of fluorescent dye-labeled HFT-T and HT-T in the dissociated xenograft tumor cells by flow cytometry. The population of human cancer cells that contain HFT-T or HT-T was identified by both EpCAM and fluorescent-labeled paclitaxel (paclitaxel-bodipy 564) encapsulated in HFT-T or HT-T. The percentage of human tumor cells containing HFT-T nanoparticles (21.8±2.9%) was three times greater than that containing HT-T nanoparticles (5.6±1.8%) (Fig. 4d), indicating that the targeted

nanoparticle is more effectively internalized into tumor cells than the non-targeted particle and correlating with its enhanced antitumor activity. Thus, the conjugation of folate to the nanoparticle greatly facilitates internalization of the nanoparticle in cancer cells *in vivo*.

In vivo antitumor efficacy and toxicity of HFT-T

We evaluated the efficacy of the HFT-T nanoparticles in promoting regression of pre-established tumors in a KB-3-1 xenograft model. Tumor-bearing mice were divided into four groups (n=7) in a way to minimize weight and tumor size differences among the groups: control group (saline), free paclitaxel group (20mg/kg), HT-T group and HFT-T group (20mg/kg paclitaxel-equivalent for nanoparticles). Therapy was continued once per week through tail vein injection for five weeks (injection time: day 1, 7, 13, 20, and 27).

All mice in the control group were sacrificed at day 15, earlier than those in the treatment groups, due to reaching the maximum tumor size according to the Institutional Animal Care and Use Committee (IACUC) guidelines. After five weeks of treatment, all mice in the remaining treatment groups were sacrificed because some mice in the free paclitaxel and HT-T groups reached IACUC endpoint volumes. A log-linear mixed model with random intercept was used to compare the mean tumor volumes between the treatment and control groups. Compared with the control group, tumor volumes in all treatment groups were significantly reduced ($p<0.0001$ for free paclitaxel, HT-T, and HFT-T each, Fig. 5a). Importantly, the tumor volume in the HFT-T-treated group was significantly smaller than that in the free paclitaxel ($p<0.0001$) or HT-T-treated ($p<0.0001$) groups, suggesting that the active targeting mechanism most likely contributes to the enhanced antitumor activity of HFT-T (supplementary Fig. 5). Indeed, after five injections (at day 33 after first injection), the tumor volume in the HFT-T-treated group ($92.9\pm78.2 mm^3$) was only 5% of that in the free paclitaxel-treated group ($1670.3\pm286.1 mm^3$).

More importantly, we observed that while treatment with free paclitaxel suppressed tumor growth initially, after three weeks of treatment, tumors no longer responded to treatments and grew rapidly. This could have resulted from the tumor cells developing drug resistance to paclitaxel. Unlike free paclitaxel, HFT-T did not show this resurgence in tumor growth rate after the same period of treatment. Three tumors (3 of 7, 42.8%) in the HFT-T-treated group shrank to a non-palpable size, leaving only scar tissue (by pathologic assessment), and these mice were cured, while no cures were attained in other treatment groups. This is strong evidence that HFT-T is much more effective than free paclitaxel in treating tumors and is less susceptible to drug resistance, which is a very common occurrence in patients clinically treated with paclitaxel.

An important consideration in nanoparticle development is the potential toxicity, especially during chronic administration. We therefore evaluated the systemic toxicity of free paclitaxel, HT-T, and HFT-T in the xenograft model. Compared with the control group, the body weights of mice in all three treatment groups were similar, indicating a negligible acute toxicity at this dose (20mg/kg paclitaxel-equivalent) (Fig. 5c). At day 34 (after 5 weeks of treatment), the histopathologic changes in major organs, such as liver, spleen, kidney, heart, and lung, from the mice in all treatment groups were examined by hematoxylin and eosin (H&E) staining. No tissue damage was observed in any organ sample collected from any treatment group, including HFT-T (Fig. 5d).

Although the accumulation of HFT-T and HT-T in the liver and kidney were relatively high, in this study no tissue damage was observed in any of the organ samples collected from any treatment group, including HFT-T and HT-T under the tested conditions. The heparin polymer that we used to synthesize the nanoparticles is biodegradable, so that HFT-T and HT-T accumulated in the liver and kidney may be degraded and eliminated through the renal

system. We continually observed a fluorescence signal in the bladder 48 hours after injection of fluorescent dye-labeled HFT-T or HT-T, implying the degradation and elimination of nanoparticles (Fig. 4a).

In the present study, we have focused on the efficacy of HFT-T nanoparticles in promoting regression of pre-established tumors in mouse models. The administration dose was determined based on previously published literature.[36] However, unlike the reported schedules for administration of free paclitaxel (daily injection for three days), our study aimed to induce tumor regression using the nanoparticles with a longer interval between two treatments, once per week (5 injections). This schedule of administration may be less toxic to animals, as demonstrated by the *in vivo* toxicity data (Fig. 5c,d), and therefore may have a better safety profile for clinical application.

In vivo effect of HFT-T on microtubule disruption and apoptosis in tumor tissues

Paclitaxel exerts its antitumor activity by binding to β-tubulin inside the lumen of the microtubule, resulting in microtubule polymerization, mitotic arrest, and apoptosis in proliferating cells. To investigate the mechanism underlying the enhanced antitumor activity of the HFT-T nanoparticle *in vivo*, we sacrificed the mice one week after the last treatment, collected tumors and examined the effect of each treatment on tubulin acetylation in xenograft tissues as a readout of drug-induced microtubule stability. Image analysis revealed a significant increase in acetylated tubulin levels in tumor xenografts from all treatment groups, free paclitaxel (132.74±28.15%), HT-T (108.35±6.34%) and HFT-T (160.26±30.14%), as compared with control (71.72±25.64%). However, the intensity of acetylated tubulin was greater in tumors treated with HFT-T than free paclitaxel ($p=0.06$) or HT-T ($p=0.001$), indicating the better efficacy of HFT-T (supplementary Fig. 4).

Drug-induced stabilization of the tumors' interphase microtubules, as evidenced by an increase in microtubule polymer mass resulting in bundling, was observed upon treatment with both HT-T and HFT-T; however HFT-T was most effective in the formation of microtubule bundles. Moreover, confocal microscopy analysis of xenograft tumor sections revealed perturbations of the microtubule cytoskeleton in HFT-T-treated animals, such as microtubule bundling and formation of aberrant mitotic spindles with mis-aligned chromosomes, indicative of effective drug-target engagement (Fig. 6a, b). To quantify the effect of each drug treatment, aberrant mitotic cells were counted and expressed as a percentage of the total cell number. The Kruskal Wallis test (one-way ANOVA) revealed that the percentage of cells arrested in mitosis was significantly greater in HFT-T-treated xenografts (8.13%) than that in control-treated xenografts (2.76%), while paclitaxel-and HT-T-treatment induced a less significant increase (5.35%) and a non-significant increase (4.66%) in aberrant mitosis, respectively.

Another interesting finding in sections of HFT-T-treated tumors was the formation of large mutinucleated cells that cannot complete cytokinesis and therefore exit mitosis with multiple N (8N and 16N) (Fig. 6b). Such large multinucleated cells were only observed in the HFT-T treatment group and not in other treatment or control groups.

Immunohistochemical analysis of Ki-67 expression and TUNEL assays revealed that HFT-T treatment resulted in greater inhibition of proliferation and induction of apoptosis in xenograft tumors. Ki-67 staining showed a trend toward lower expression in HFT-T-treated tumors (weighted index of Ki67: 0.61±0.35) than in the control (1.25±0.31), paclitaxel (1.16±0.11), or HT-T-treated (1.38±0.190) groups (Fig. 6a). The level of apoptosis in tumors of the HFT-T (0.046±0.005) and HT-T (0.049±0.006) groups was slightly greater than in the control (0.035±0.01) and free paclitaxel (0.038±0.008) groups (Fig. 6a). Together, these data indicate that HFT-T treatment was more efficacious in inducing

microtubule stabilization, mitotic arrest and reducing proliferation than the other tested treatments, presumably by specific delivery of paclitaxel into FR-positive tumors.

CONCLUSIONS

In summary, our novel FR-targeted nanoparticle HFT-T significantly facilitated the specific delivery of paclitaxel to FR-positive tumor cells and demonstrated strongly enhanced *in vivo* efficacy when compared with free paclitaxel. This leads us to believe that using targeted nanoparticles as a specific and efficient drug delivery system is a promising strategy to treat human cancers and other diseases.

MATERIALS AND METHODS

Preparation of Nanoparticles

In order to obtain the targeted nanoparticles, heparin bearing paclitaxel and folic acid in the side-chains was synthesized first. The synthesis of the targeted HFT conjugate (polymer **4)** is outlined in Fig. 1A. The following is an outline of the synthesis process, the details of which are presented in the supplemental information. Heparin was pre-treated with the ion exchange resin, Dowex-50 (H^+ form) and then mixed with an excess amount of tributylamine to allow for the modification reactions of polymer **1** in dimethylformamide (DMF).[38, 39] The resulting polymer **2** (1.0g), and succinic anhydride (0.167g), were allowed to stir in DMF at room temperature overnight in the presence of 4-(dimethylamino)pyridine (DMAP) (1.67mg, 1% (w/w) of succinic anhydride). The product, polymer **3**, was purified by dialysis (MWCO = 3,500) against water for 3 days and then lyophilized. Paclitaxel (60mg) and NH_2-modified folic acid (11mg) were chemically conjugated onto polymer **3** (200mg), through a two-step coupling reaction.[40, 41] After dialysis (MW = 3,500) against water for 3 days and lyophilization, the final polymer **4**, was obtained as a light yellow colored powder. Using the same process, paclitaxel only (without folic acid) was chemically conjugated onto polymer **3** to yield the heparin-paclitaxel conjugate (HT).

In order to prepare the drug-loaded nanoparticles (HFT-T and HT-T), polymer **4** (100mg, paclitaxel content: 15% w/w) and free paclitaxel (15mg) were dissolved in DMSO (3ml). The solution was added into $NaHCO_3$ (0.1M, 20ml) dropwise. DMSO was removed by dialysis. The resulting solution was filtered by using a 0.2 μm membrane, and concentrated on an Ultra-Centrifugal Filter (MW = 5000).

The final content of paclitaxel in the stock solution was determined by UV absorption. The surface morphology and size of nanoparticles were investigated by transmission electron microscopy (TEM, Hitachi, Japan). The dynamic size of nanoparticle was measured using a Dynamic Light Scattering Detector (DLS, Brookhaven Instruments, Holtsville, NY). The anticoagulant activities of HFT-T were determined by FXa-dependent coagulant assay using Coatest Heparin according to the manufacturer's instructions.

In vitro cytotoxicity assays

To study the effect of HFT-T on clonogenicity, we used human head and neck cell lines KB-3-1 and Tu212, which express high and undetectable levels of FR, respectively. The cells (1.0×10^3/well) were seeded into 6-well plates in triplicate. After 24 hours, 2.5nM paclitaxel or paclitaxel-equivalent dose of HFT-T or HT-T was added, and medium was changed every three days. The cells were incubated in the presence of the drugs for two weeks to form colonies. The cell colonies were stained in crystal violet (0.5%), and then counted under a microscope. The experiment was repeated three times.

Uptake and intracellular localization of HFT-T in KB-3-1 cells

Fluorescent dye-labeled HFT-T or HT-T was prepared by encapsulation of paclitaxel-oregon green 488 (supplementary information). KB-3-1 or Tu212 cells were incubated with HT-T or HFT-T (containing 10nM paclitaxel-oregeon green 488) for two hours at 37°C, and then washed three times with PBS and analyzed by FACS or alternatively fixed with 4% paraformaldehyde. For confocal microscopy, cells were mounted using DAPI-containing reagent (Invitrogen, Carlsbad CA).

To knockdown FR expression, Smartpool FR siRNA that targets the FR (Dharmacon Lafayette, CO) was transfected into KB-3-1 cells. Transfection of siRNA was performed with RNAiFect transfection reagent (Qiagen, Valencia, CA). KB-3-1 cells were transfected with 200nM FR siRNA or control siRNA. Forty-eight hours later, the transfection medium was replaced by normal medium for HFT-T uptake study. Fifty micrograms of whole cell lysate for each sample were also made for immunoblotting analysis to detect gene-silencing efficiency. All experiments were repeated thrice.

In vivo biodistribution Assay

All animal experiments were approved by the IACUC of Emory University. KB-3-1 cells (1.0×10^6) were injected s.c. into the low back of 4-5 week-old female nude mice, and allowed to grow for 10 days post-inoculation with tumor size of about 400 mm^3 (n=3 for each group). Then 100μl of near infrared dye (Cy5.5)-labeled HFT-T and HT-T nanoparticles (containing 20μM of cy5.5) (supplementary information) was injected i.v. to mice. Images were taken at 1h, 24h, and 48h after injection using the Kodak imaging station IS2000MM (Eastman Kodak company, New Haven, CT). Forty-eight hours after injection, the mice were sacrificed. The tissues including tumor, liver, heart, lung, spleen, and kidney were collected and analyzed by using Kodak 1DTM 3.6.3 Network software.

Quantitative analysis of HFT-T uptake in tumor cells *in vivo*

Fluorescent dye-labeled (paclitaxel-bodipy 564) HFT-T or HT-T (200μl 7mg/ml paclitaxel-equivalent dose) (supplementary information) was injected i.v. into mice bearing KB-3-1 tumors (about 400mm^3; n=3 per group). Twenty-four hours later, the mice were sacrificed, and tumors were excised, mechanically fragmented, and treated sequentially with disaggregation buffer (0.1% collagenase type IV and 0.003% DNase I in Hank's buffered salt solution) for 1 hour at 37°C. Following centrifugation at 4°C, cell pellets were gently resuspended in cold PBS containing 0.1% bovine serum albumin. To differentiate cancer cells from cells of the mouse host, the cell suspension was stained with FITC-conjugated EpCAM antibody (Miltenyi Biotec, CA) on ice for 30 minutes. The cells were washed with cold BSA-PBA-azide, and analyzed by flow cytometry.[37]

In vivo anti-tumor efficacy Assay

KB-3-1 cells (1.0×10^6) were injected s.c. into 4-5 week-old female nude mice. When the tumors had developed to about 100mm^3, the mice were divided into four groups (n=7) in a way to minimize weight and tumor size differences among the groups: control group treated with saline, free paclitaxel group (20mg/kg), HT-T group, and HFT-T group (20mg/kg paclitaxel-equivalent for nanoparticles). Therapy was continued once per week through tail vein injection for five weeks. The body weight and tumor size were measured three times per week. The tumor volume was calculated using the formula: $V = \pi/6 \times \text{larger diameter} \times (\text{smaller diameter})$.[2] After five weeks treatment, tumor and organ tissues (liver, heart, lung, spleen, and kidney) were collected for H&E staining and immunostaining analyses.

Acetylated tubulin and vimentin double staining

Double staining for acetylated tubulin and vimentin was performed using paraffin-embedded mouse xenograft tissue. The sections were incubated in 2.8 μg/ml monoclonal anti-acetylated tubulin (Sigma, St. Louis, MO) for 3 hours followed by incubation with biotinylated antimouse secondary antibody (Vector labs, Burlingame, CA; in 1:200 dilution) for 1 hour. Detection was performed with Streptavidin-HRP D (Ventana Medical Systems), followed by incubation with Tyramide-Alexa Fluor 568 (Invitrogen, Carlsbad CA). After saturating the tissue sections with anti-acetylated tubulin primary antibody, the sections were blocked in mouse IgG blocking reagent, followed by incubation with 0.1 μg/ml monoclonal anti-vimentin (Vector Laboratories, Burlingame, CA) for 3 hours and 1 hour incubation with a biotinylated mouse secondary antibody. The detection was performed with Streptavidin-HRP D, followed by incubation with Tyramide-Alexa Fluor 488 (Invitrogen, Carlsbad CA). Then, the sections were stained with DAPI or sytox green and mounted.

The fluorescence intensity of acetylated tubulin was recorded using the Zeiss Axiovision Software and further normalized to the fluorescence intensity of vimentin staining. Three representative images were taken for each sample. The percentage of acetylated tubulin staining (both human and mouse) were calculated and normalizing to vimentin staining. DAPI staining was used to obtain approximately the same number of cells for all the samples.

Immunohistochemistry and TUNEL Assay

Immunohistochemical analysis for Ki-67 staining on paraffin-embedded mouse xenograft tissue was performed. Tissue sections were incubated with mouse anti-human Ki-67 (prediluted; Invitrogen, Carlsbad, CA) overnight at 4°C. The slides were stained with 3,3-diaminobenzidine (Vector Laboratories, Burlingame, CA) and counterstained with hematoxylin (Vector Laboratories, Burlingame, CA). TUNEL assay was performed by immunofluorescence using the same specimens as above following the procedure provided by the manufacturer (Promega, Madison, WI). The slides were counterstained with DAPI (Vector Laboratories, Burlingame, CA).

The intensity of Ki-67 staining was measured using a scale (0=no expression, 1+=weak expression, 2+=moderate expression, and 3+=strong expression) and quantified as Weighted Index (WI=% positive staining in tumor intensity score). An average of the ten readings was used for statistical analysis. For TUNEL assay, the total cell number and the positive cell number in the same area were counted for five random areas; the result was presented as an average ratio of positive cell number out of total cell number.

Supplementary Material

Refer to Web version on PubMed Central for supplementary material.

Acknowledgments

We thank Dr. Anthea Hammond for her critical reading of the manuscript.

Financial support:

This work was supported by a SPORE grant (P50CA128613-02S1) for Dong M Shin, a CCNE grant (U54CA119338-04) for Shuming Nie, and the Georgia Cancer Coalition Distinguished Scholar Award for Dong M. Shin, Shuming Nie, and Zhou (Georgia) Chen.

References

1. Rowinsky EK, Cazenave LA, Donehower RC. Taxol: A Novel Investigational Antimicrotubule Agent. J Natl Cancer Inst. 1990; 82:1247–1259. [PubMed: 1973737]
2. Lopes NM, Adams EG, Pitts TW, Bhuyan BK. Cell Kill Kinetics and Cell Cycle Effects of Taxol on Human and Hamster Ovarian Cell Lines. Cancer Chemother Pharmacol. 1993; 32:235–242. [PubMed: 8098996]
3. Donehower RC, Rowinsky EK, Grochow LB, Longnecker SM, Ettinger DS. Phase I Trial of Taxol in Patients with Advanced Cancer. Cancer Treat Rep. 1987; 71:1171–1177. [PubMed: 2891441]
4. Weiss RB, Donehower RC, Wiernik PH, Ohnuma T, Gralla RJ, Trump DL, Baker JR Jr. Van Echo DA, Von Hoff DD, Leyland-Jones B. Hypersensitivity Reactions from Taxol. J Clin Oncol. 1990; 8:1263–1268. [PubMed: 1972736]
5. Chu Q, Vincent M, Logan D, Mackay JA, Evans WK. Taxanes as First-Line Therapy for Advanced Non-Small Cell Lung Cancer: A Systematic Review and Practice Guideline. Lung Cancer. 2005
6. Brannon-Peppas L, Blanchette JO. Nanoparticle and Targeted Systems for Cancer Therapy. Adv Drug Deliv Rev. 2004; 56:1649–1659. [PubMed: 15350294]
7. Taxol (Paclitaxel) Injection. Bristol-Myers Squibb Co.; Princeton (Nj): Mar.. 2003 Package Insert
8. Gradishar WJ, Tjulandin S, Davidson N, Shaw H, Desai N, Bhar P, Hawkins M, O'Shaughnessy J. Phase Iii Trial of Nanoparticle Albumin-Bound Paclitaxel Compared with Polyethylated Castor Oil-Based Paclitaxel in Women with Breast Cancer. J Clin Oncol. 2005; 23:7794–7803. [PubMed: 16172456]
9. Guillemard V, Uri Saragovi H. Prodrug Chemotherapeutics Bypass P-Glycoprotein Resistance and Kill Tumors in Vivo with High Efficacy and Target-Dependent Selectivity. Oncogene. 2004; 23:3613–3621. [PubMed: 15034547]
10. Guillemard V, Saragovi HU. Novel Approaches for Targeted Cancer Therapy. Curr Cancer Drug Targets. 2004; 4:313–326. [PubMed: 15180497]
11. Pechar M, Ulbrich K, Subr V, Seymour LW, Schacht EH. Poly(Ethylene Glycol) Multiblock Copolymer as a Carrier of Anti-Cancer Drug Doxorubicin. Bioconjug Chem. 2000; 11:131–139. [PubMed: 10725088]
12. Mansour AM, Drevs J, Esser N, Hamada FM, Badary OA, Unger C, Fichtner I, Kratz F. A New Approach for the Treatment of Malignant Melanoma: Enhanced Antitumor Efficacy of an Albumin-Binding Doxorubicin Prodrug That Is Cleaved by Matrix Metalloproteinase 2. Cancer Res. 2003; 63:4062–4066. [PubMed: 12874007]
13. Lu ZR, Gao SQ, Kopeckova P, Kopecek J. Modification of Cyclosporin a and Conjugation of Its Derivative to Hpma Copolymers. Bioconjug Chem. 2001; 12:129–133. [PubMed: 11170375]
14. Kong G, Anyarambhatla G, Petros WP, Braun RD, Colvin OM, Needham D, Dewhirst MW. Efficacy of Liposomes and Hyperthermia in a Human Tumor Xenograft Model: Importance of Triggered Drug Release. Cancer Res. 2000; 60:6950–6957. [PubMed: 11156395]
15. Li C. Poly(L-Glutamic Acid)--Anticancer Drug Conjugates. Adv Drug Deliv Rev. 2002; 54:695–713. [PubMed: 12204599]
16. Sudimack J, Lee RJ. Targeted Drug Delivery Via the Folate Receptor. Adv Drug Deliv Rev. 2000; 41:147–162. [PubMed: 10699311]
17. Ni S, Stephenson SM, Lee RJ. Folate Receptor Targeted Delivery of Liposomal Daunorubicin into Tumor Cells. Anticancer Res. 2002; 22:2131–2135. [PubMed: 12174894]
18. Backer MV, Gaynutdinov TI, Aloise R, Przekop K, Backer JM. Engineering S-Protein Fragments of Bovine Ribonuclease a for Targeted Drug Delivery. Protein Expr Purif. 2002; 26:455–461. [PubMed: 12460770]
19. Backer MV, Aloise R, Przekop K, Stoletov K, Backer JM. Molecular Vehicles for Targeted Drug Delivery. Bioconjug Chem. 2002; 13:462–467. [PubMed: 12009934]
20. Davis ME, Chen ZG, Shin DM. Nanoparticle Therapeutics: An Emerging Treatment Modality for Cancer. Nat Rev Drug Discov. 2008; 7:771–782. [PubMed: 18758474]
21. Wang X, Yang L, Chen ZG, Shin DM. Application of Nanotechnology in Cancer Therapy and Imaging. CA Cancer J Clin. 2008; 58:97–110. [PubMed: 18227410]

22. Cho K, Wang X, Nie S, Chen ZG, Shin DM. Therapeutic Nanoparticles for Drug Delivery in Cancer. Clin Cancer Res. 2008; 14:1310–1316. [PubMed: 18316549]
23. Elnakat H, Ratnam M. Role of Folate Receptor Genes in Reproduction and Related Cancers. Front Biosci. 2006; 11:506–519. [PubMed: 16146749]
24. Kalli KR, Oberg AL, Keeney GL, Christianson TJ, Low PS, Knutson KL, Hartmann LC. Folate Receptor Alpha as a Tumor Target in Epithelial Ovarian Cancer. Gynecol Oncol. 2008; 108:619–626. [PubMed: 18222534]
25. Dainty LA, Risinger JI, Morrison C, Chandramouli GV, Bidus MA, Zahn C, Rose GS, Fowler J, Berchuck A, Maxwell GL. Overexpression of Folate Binding Protein and Mesothelin Are Associated with Uterine Serous Carcinoma. Gynecol Oncol. 2007; 105:563–570. [PubMed: 17400285]
26. Saba NF, Wang X, Muller S, Tighiouart M, Cho K, Nie S, Chen Z, Shin DM. Examining Expression of Folate Receptor in Squamous Cell Carcinoma of the Head and Neck as a Target for a Novel Nanotherapeutic Drug. Head Neck. 2009; 31:475–481. [PubMed: 19072997]
27. Hartmann LC, Keeney GL, Lingle WL, Christianson TJ, Varghese B, Hillman D, Oberg AL, Low PS. Folate Receptor Overexpression Is Associated with Poor Outcome in Breast Cancer. Int J Cancer. 2007; 121:938–942. [PubMed: 17487842]
28. Iwakiri S, Sonobe M, Nagai S, Hirata T, Wada H, Miyahara R. Expression Status of Folate Receptor Alpha Is Significantly Correlated with Prognosis in Non-Small-Cell Lung Cancers. Ann Surg Oncol. 2008; 15:889–899. [PubMed: 18181001]
29. Lee KW, Yoon JJ, Lee JH, Kim SY, Jung HJ, Kim SJ, Joh JW, Lee HH, Lee DS, Lee SK. Sustained Release of Vascular Endothelial Growth Factor from Calcium-Induced Alginate Hydrogels Reinforced by Heparin and Chitosan. Transplant Proc. 2004; 36:2464–2465. [PubMed: 15561282]
30. Rajangam K, Behanna HA, Hui MJ, Han X, Hulvat JF, Lomasney JW, Stupp SI. Heparin Binding Nanostructures to Promote Growth of Blood Vessels. Nano Lett. 2006; 6:2086–2090. [PubMed: 16968030]
31. Meister B, Kropshofer G, Klein-Franke A, Strasak AM, Hager J, Streif W. Comparison of Low-Molecular-Weight Heparin and Antithrombin Versus Antithrombin Alone for the Prevention of Symptomatic Venous Thromboembolism in Children with Acute Lymphoblastic Leukemia. Pediatr Blood Cancer. 2008; 50:298–303. [PubMed: 17443678]
32. Icli F, Akbulut H, Utkan G, Yalcin B, Dincol D, Isikdogan A, Demirkazik A, Onur H, Cay F, Buyukcelik A. Low Molecular Weight Heparin (Lmwh) Increases the Efficacy of Cisplatinum Plus Gemcitabine Combination in Advanced Pancreatic Cancer. J Surg Oncol. 2007; 95:507–512. [PubMed: 17192920]
33. Collen A, Smorenburg SM, Peters E, Lupu F, Koolwijk P, Van Noorden C, van Hinsbergh VW. Unfractionated and Low Molecular Weight Heparin Affect Fibrin Structure and Angiogenesis in Vitro. Cancer Res. 2000; 60:6196–6200. [PubMed: 11085545]
34. Vlodavsky I, Friedmann Y, Elkin M, Aingorn H, Atzmon R, Ishai-Michaeli R, Bitan M, Pappo O, Peretz T, Michal I, et al. Mammalian Heparanase: Gene Cloning, Expression and Function in Tumor Progression and Metastasis. Nat Med. 1999; 5:793–802. [PubMed: 10395325]
35. Freeman C, Browne AM, Parish CR. Evidence That Platelet and Tumour Heparanases Are Similar Enzymes. Biochem J. 1999; 342(Pt 2):361–368. [PubMed: 10455023]
36. Kim SC, Kim DW, Shim YH, Bang JS, Oh HS, Wan Kim S, Seo MH. In Vivo Evaluation of Polymeric Micellar Paclitaxel Formulation: Toxicity and Efficacy. J Control Release. 2001; 72:191–202. [PubMed: 11389998]
37. Kirpotin DB, Drummond DC, Shao Y, Shalaby MR, Hong K, Nielsen UB, Marks JD, Benz CC, Park JW. Antibody Targeting of Long-Circulating Lipidic Nanoparticles Does Not Increase Tumor Localization but Does Increase Internalization in Animal Models. Cancer Res. 2006; 66:6732–6740. [PubMed: 16818648]
38. Barzu T, Level M, Petitou M, Lormeau JC, Choay J, Schols D, Baba M, Pauwels R, Witvrouw M, De Clercq E. Preparation and Anti-Hiv Activity of O-Acylated Heparin and Dermatan Sulfate Derivatives with Low Anticoagulant Effect. J Med Chem. 1993; 36:3546–3555. [PubMed: 8246223]

39. Stevens MM, Allen S, Davies MC, Roberts CJ, Schacht E, Tendler SJB, VanSteenkiste S, Williams PM. The Development, Characterization, and Demonstration of a Versatile Immobilization Strategy for Biomolecular Force Measurements. Langmuir. 2002; 18:6659–6665.

40. Yu MK, Lee DY, Kim YS, Park K, Park SA, Son DH, Lee GY, Nam JH, Kim SY, Kim IS, et al. Antiangiogenic and Apoptotic Properties of a Novel Amphiphilic Folate-Heparin-Lithocholate Derivative Having Cellular Internality for Cancer Therapy. Pharm Res. 2007; 24:705–714. [PubMed: 17318418]

41. Aronov O, Horowitz AT, Gabizon A, Gibson D. Folate-Targeted Peg as a Potential Carrier for Carboplatin Analogs. Synthesis and in Vitro Studies. Bioconjug Chem. 2003; 14:563–574. [PubMed: 12757380]

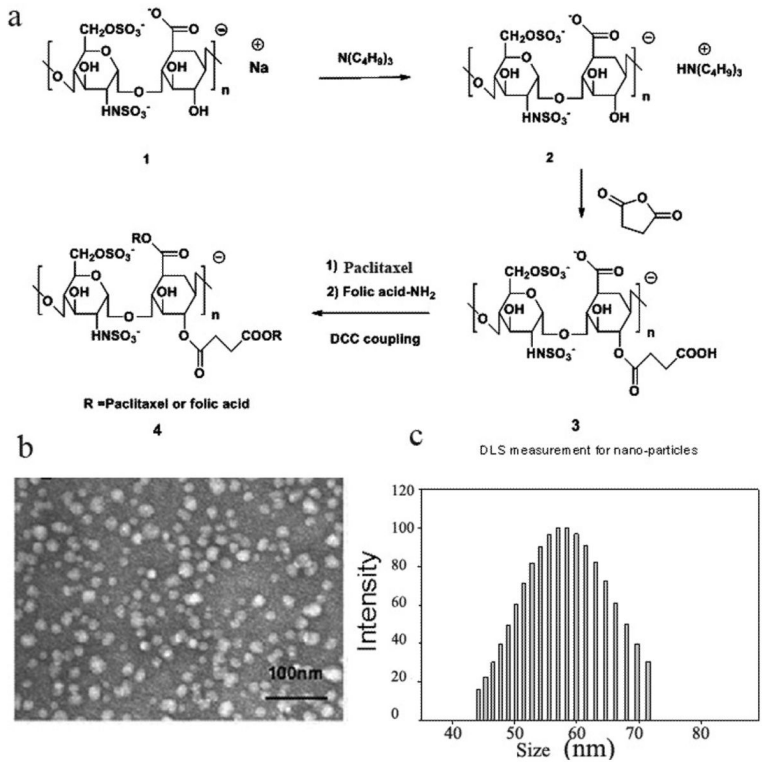

Fig. 1.

Synthesis and characterization of heparin-folic acid-paclitaxel nanoparticles loaded with paclitaxel (HFT-T). (a) Diagram of conjugation reaction for heparin-folic acid-paclitaxel (HFT) conjugate. (b) TEM image of HFT-T nanoparticles. (c) DLS measurement of HFT-T nanoparticles, the graph shows size distribution of HFT-T nanoparticle in water.

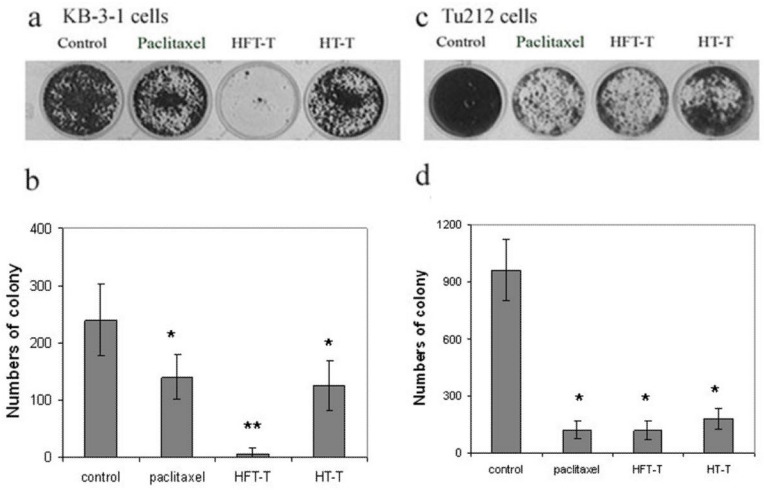

Fig. 2.

Effect of HFT-T on colony formation. KB-3-1 (a, b) and Tu212 (c, d) cells were treated with 2.5nM paclitaxel or paclitaxel-equivalent dose of HFT-T or HT-T for 2 weeks. Colony-forming capability was markedly suppressed by HFT-T treatment when compared with all other treatments in KB-3-1 cells, but was similar in Tu212 cells. (*$p < 0.05$ and **$p<0.001$ compared with control, results are mean ± s.e.).

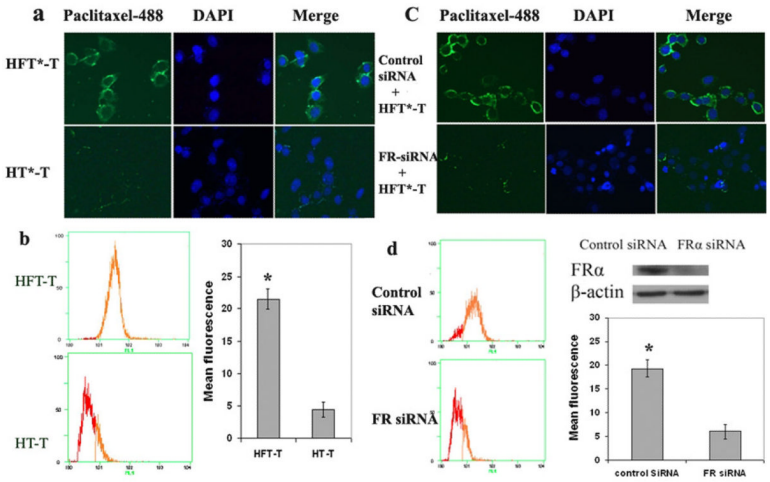

Fig. 3.

Specificity of tumor cell targeting of HFT-T. (a) Confocal images show KB-3-1 cell uptake of HFT-T or HT-T after 2 hours incubation. (b) Uptake of HFT-T or HT-T by KB-3-1 cells was evaluated by flow cytometry. Left panel shows the mean fluorescence in cells after 2 hours exposure to HFT-T or HT-T at 37°C. (c) Confocal images show that the uptake of HFT-T in KB-3-1 cells treated with FR siRNA (FR-knockout) was decreased compared with that in KB-3-1 cells treated with the control siRNA. (d) Immunoblotting analysis was used to examine level of FRα protein in KB-3-1 cells after treatment with the siRNA for FRα or control siRNA. Uptake of HFT-T by FR knockout KB-3-1 cells or control KB-3-1 cells was analyzed by flow cytometry. (*$p < 0.05$, results are mean ± s.e.).

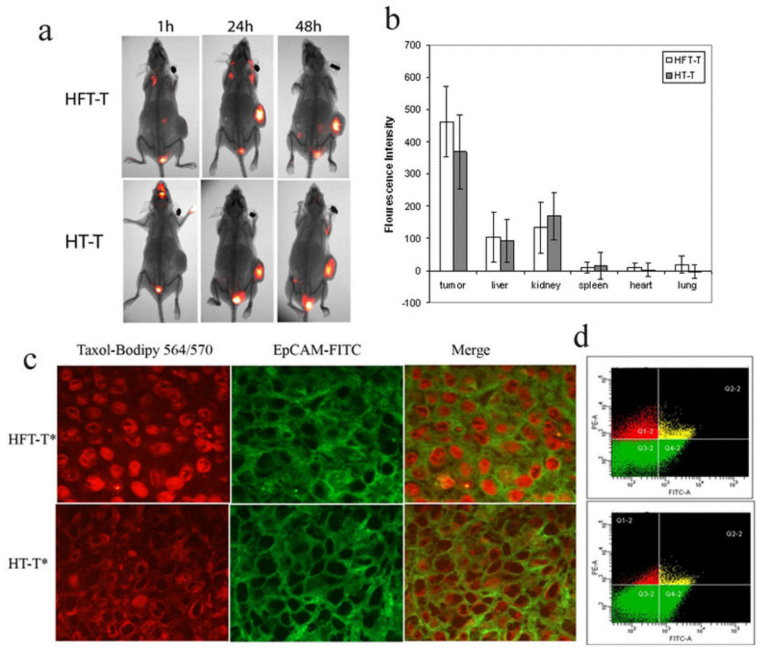

Fig. 4.

In vivo distribution of HFT-T in KB-3-1 tumor-bearing mice. Near infrared dye (cy5.5)-labeled HFT-T or HT-T was injected i.v. into KB-3-1 tumor-bearing mice. (a) Imaging of mice at 1h, 24h, and 48h after injection. (b) Biodistribution of HFT-T and HT-T in major organs at 48 hours after injection. (c) The cellular internalization of HFT-T versus HT-T in KB-3-1 xenografts 24 hours after injection (i.v.). HFT-T showed marked internalization in KB-3-1 cells identified by human EpCAM expression (green). In contrast, HT-T showed much less internalization by KB-3-1 cells and was predominantly found in the extracellular space. (d) Flow cytometry analyses of cells obtained from disaggregated KB-3-1 xenografts 24 hours after i.v. injection of HFT-T or HT-T. Two-dimensional event density plots of disaggregated tumor cell suspensions from animals injected with HFT-T or HT-T. The cells were stained with anti-EpCAM Ab-FITC conjugate to identify human cancer cells. The cells in Q4-2 and Q2-2 were human tumor cells (EpCAM positive), the cells in Q1-2 and Q2-2 contained nanoparticles (bodipy 564 positive), and the cells in Q2-2 were human tumor cells containing nanoparticles (double positive).

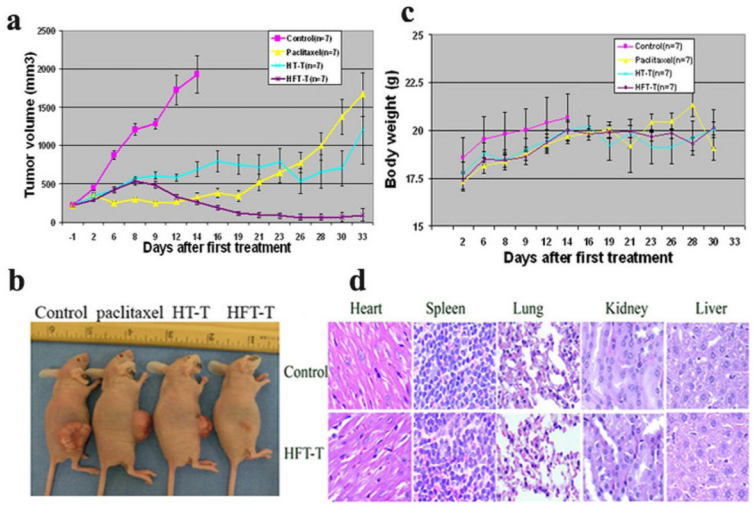

Fig. 5.

Antitumor effect of HFT-T nanoparticle in animal model. (a). The growth curve of KB-3-1 xenografts showed that all the treatment groups including free paclitaxel, HT-T, and HFT-T significantly inhibited the growth of tumor as compared with the control ($p<0.0001$ for each treatment). Although the tumor volumes were similar in HT-T and free paclitaxel-treated groups ($p=0.608$), FR-targeted HFT-T more potently reduced tumor growth than free paclitaxel ($p<0.0001$). After 5 injections, the average tumor volumes in paclitaxel, HT-T, and HFT-T treatment groups were 1670.3 ± 286.1 mm^3, 1211.3 ± 448.1 mm^3, and 92.9 ± 78.2 mm^3, respectively. (b) A representative mouse from each group. (c) The body weights of the mice in all groups. (d) Representative images of H&E organ staining from control and HFT-T-treated mice (magnification 200).

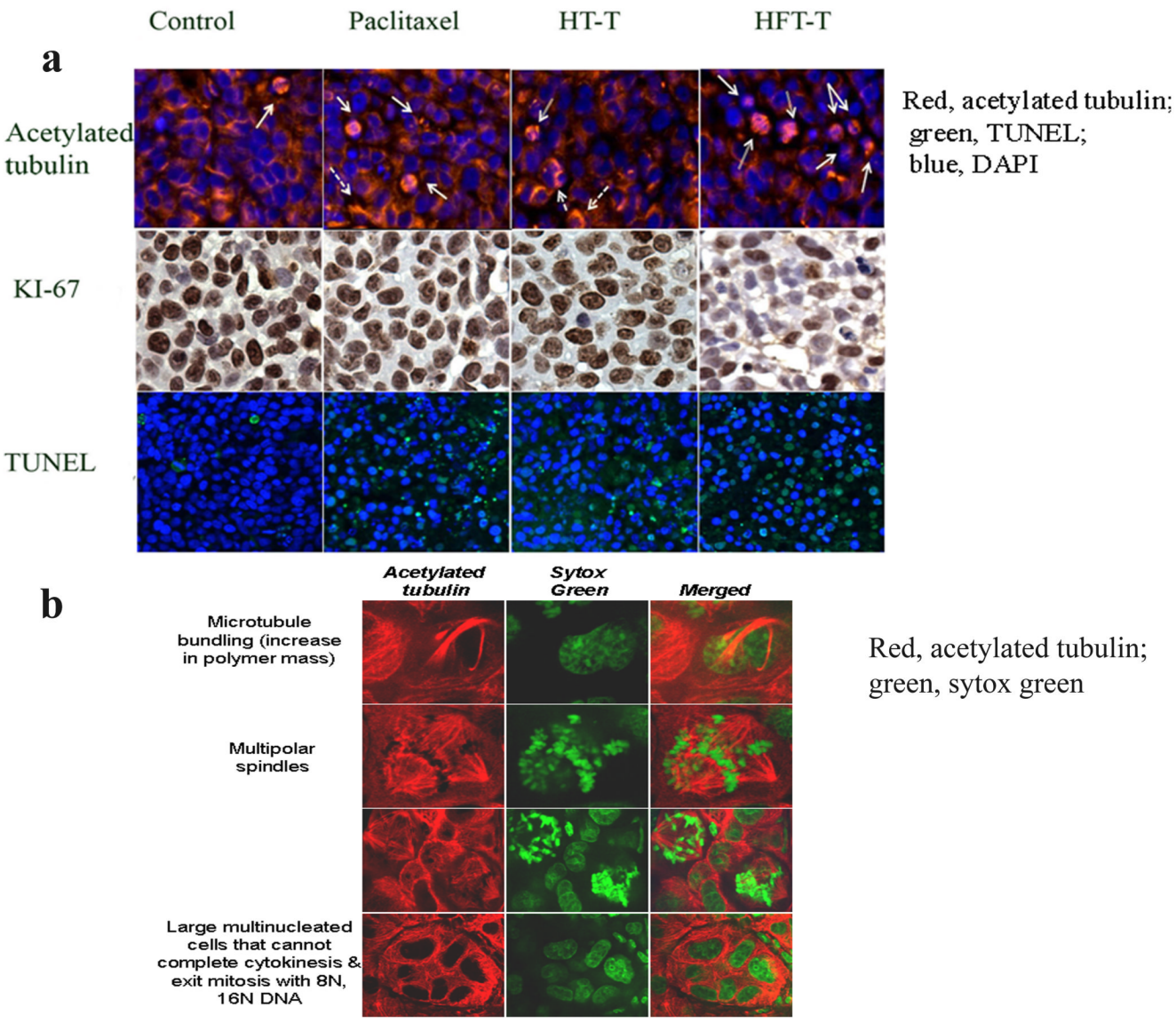

Fig. 6.

Effects of HFT-T on cell division, proliferation, and apoptosis. (a) Paraffin-embedded tissue sections from different treatment groups were immunostained with anti-acetylated tubulin to detect acetylated tubulin, anti-KI-67 for cell proliferation, and TUNEL staining for the detection of apoptotic cells. Acetylated-α-tubulin in red; apoptotic cells are shown in green; DNA counterstained with DAPI in blue. Arrows point to mitotic figures. Arrow in control: normal dividing cell in anaphase; Arrow in treatment groups: aberrant mitotic arrest; Dashed arrow: microtubule bundling; Two-line arrow: multipolar spindles. (b) Confocal microscopy analysis revealed perturbations of the microtubule cytoskeleton in the HFT-T-treated animals, including microtubule bundling (tubulin in red), formation of aberrant mitotic spindles with mis-aligned chromosomes (DNA in blue), and formation of large multinucleated cells.